Multistep active screen plasma co-alloying the treatment of metallic bipolar plates

Kaijie Lin, Xiaoying Li, Hanshan Dong & Dongdong Gu

Published online: 20 Jan 2020.

Submit your article to this journal ⬀

Article views: 8

View related articles ⬀

View Crossmark data ⬀

The Institute of Materials, Minerals and Mining

Taylor & Francis
Taylor & Francis Group

Check for updates

Multistep active screen plasma co-alloying the treatment of metallic bipolar plates

Kaijie Lin[a,b,c], Xiaoying Li[d], Hanshan Dong[d] and Dongdong Gu[a,b,e]

[a]College of Materials Science and Technology, Nanjing University of Aeronautics and Astronautics, Nanjing, People's Republic of China; [b]Jiangsu Provincial Engineering Laboratory for Laser Additive Manufacturing of High-Performance Metallic Components, Nanjing University of Aeronautics and Astronautics, Nanjing, People's Republic of China; [c]Key Laboratory of Materials Preparation and Protection for Harsh Environment (Nanjing University of Aeronautics and Astronautics), Ministry of Industry and Information Technology, Nanjing, People's Republic of China; [d]School of Metallurgy and Materials, The University of Birmingham, Birmingham, UK; [e]National Key Laboratory of Science and Technology on Helicopter Transmission, Nanjing University of Aeronautics and Astronautics, Nanjing, People's Republic of China

ABSTRACT

Active screen plasma (ASP) surface treatments have been widely utilized to improve surface performances of stainless steel in various applications. In our previous research, active screen plasma nitriding (ASPN) and active screen plasma co-alloying processes have been successfully employed to modify 316L stainless steel for the application of proton exchange membrane (PEM) fuel cell bipolar plates. In this study, a multistep active screen plasma co-alloying surface treatment with niobium and nitrogen was proposed to produce a tailored layer structure on the surface of 316L stainless steel. By tailoring the applied bias of step, single-layer and duplex-layer structures can be formed on the surface of 316L stainless steel. Performance tests showed that the sample with a duplex-layer structure exhibited improved interfacial contact conductivity and higher corrosion potential than the sample with a single-layer structure, indicating the feasibility of this multistep active screen plasma co-alloying surface treatment for PEM fuel cell bipolar plate application.

Introduction

The stainless steel is the most promising alternative material to the brittle and high-cost graphite for the application of bipolar plates in proton exchange membrane fuel cells, due to its low-cost, great mechanical behaviour and good corrosion resistance [1]. The good corrosion resistance of stainless steel is contributed by the formation of a dense oxide protect film on its surface. It is well known that the bipolar plate is a multi-functional component in the fuel stack and its most important functions are electrical connector and current collector. The formation of an insulating oxide film on the stainless steel surface would significantly increase the electrical resistance and thus seriously degrade the fuel cell output power density. Therefore, it is a timely task from both a scientific and technological point of view to modify the surface of stainless steel to enhance the surface conductivity and, in the meantime, maintain the good corrosion resistance.

In recent years, surface nitriding techniques have been widely utilized to modify the surface of stainless steel bipolar plates. The high temperature gas nitriding was first applied by Wang et al. [2,3]. Although, the surface electrical conductivity could be enhanced, the formation of Cr precipitation led to the degradation of corrosion resistance. The low temperature plasma nitriding could avoid the formation of Cr precipitation, thus maintain or even slightly improve the corrosion resistance [4]. However, the surface electrical conductivity cannot meet the requirement of the Department of Energy (DOE) target, because the passive film still formed on the surface of nitrided stainless steel [5,6].

Active screen plasma nitriding [7–9] is a newly developed plasma nitriding technique and possesses its potential in modifying the 316 stainless steel for the application of bipolar plates. In previous research [10], the deposition layer, unique to active screen plasma treatment, was found to play an important role in surface properties. However, like other surface nitriding treatments, the surface electrical conductivity cannot satisfy the requirement. In order to further enhance the surface electrical conductivity, the active screen plasma nitriding has been combined with the surface niobium-alloying technique, namely active screen plasma alloying with nitrogen and niobium (ASPA(N + Nb)) [11]. Results showed that by controlling the applied bias of the nitriding process, the microstructures of the modified surface can be tailored: when low bias was applied, a duplex-layer structure,

Table 1. The chemical composition of 316 stainless steel.

Element	C	Cr	Mn	Mo	Ni	S	P	Si	Fe
Content (wt-%)	0.06	17.20	1.30	2.20	11.70	0.014	0.026	0.60	66.90

consisting a very thin niobium-containing deposition layer (∼0.2 μm) and a nitrogen-expanded austenite layer (S-phase) (∼6.3 μm), was produced; when high bias was applied, a niobium nitride single layer (0.4–0.6 μm) was produced. The interfacial contact resistance of the duplex-layer structure surface was much lower than the normal ASPN-treated surface and slightly lower than the niobium nitride single-layer structure. However, the corrosion resistance of the duplex structure surface was worse than the niobium nitride single-layer structure due to the relatively thin niobium nitride layer.

In this paper, multistep ASPA(N + Nb) treatments have been conducted to produce a duplex-layer structure surface, consisting of a thick niobium nitride layer and an S-phase layer, in order to take full advantage of the two layers and further improve the surface electrical conductivity. The microstructure and composition of the modified surface were fully investigated by the means of scanning electron microscopy (SEM), energy-dispersive X-ray spectroscopy (EDS), glow discharge optical emission spectroscopy (GDOES) and transmission electron microscopy (TEM). The surface electrical conductivity and corrosion resistance were evaluated by means of interfacial contact resistance (ICR) tests and potentio-dynamic polarization tests, respectively.

Material and methods

Material and ASPA(N + Nb) treatment

The commercial austenitic 316 stainless steel was selected as the substrate and its chemical composition is listed in Table 1. Coupon samples were first cut from long hot rolled bar into 70 mm short bars using metal cutting band saw and then further cut into coupons using the Struers Accutom-5 cutting machine with an SiC cutting wheel. The final size of the coupon samples was 25.4 mm (1 inch) in diameter and 6 mm in thickness. The untreated sides of the samples were wet-ground using SiC-grinding paper from grit #120 up to grit #1200. The treated sides were first wet-ground up to grit #1200 and subsequently polished using diamond pastes from 9 μm down to 1 μm. The grinding and polishing were all conducted using the Struers LaboPol-5 Grinding and Polishing Machine. Before treatments, samples were washed using cotton dipped with detergent, ultrasonically cleaned in acetone for 5 min and finally dried in flowing hot air. The active screen plasma alloying treatments were conducted in an AS Plasma Metal 75 kVA + 15 kVA industrial scale unit and its details can be found in the

previous paper [11]. The parameter settings of the multistep treatments are presented in Table 2. The other parameters were set constantly during two steps such as temperature 450°C, pressure 0.75 mbar, gas mixture 25% N_2 + 75% H_2.

Surface layer characterization

The surface and cross-sectional morphologies of the ASPA(N + Nb)-treated 316 stainless steel were observed by a Jeol 7000 field emission SEM unit. The surface chemical composition was measured by an Oxford Instrument Inca EDS equipped in the SEM unit, and the element depth profiles were conducted by a Leco GDS-750 GDOES unit. The surface roughness was measured by an AMBIOS XP-200 Stylus Profiler, the reported values of each sample were the average of at least three measurements and the measured sites were randomly chose. The phase constituent was characterized by XRD (Bruker D8 Advance) with Cu Kα radiation ($λ = 0.154$ nm). The cross-sectional TEM samples were cut from the treated 316 stainless steel sample and first mechanically ground to around 50 μm. The final thinning process was conducted in a FEI Quanta 3D FEG, using focused ion beam. Before thinning, a platinum coating was deposited on the surface of the thinning area. A JEOL 2100 200 kV LaB6 TEM with Oxford Inca EDS was employed to conduct the TEM analysis with an operating voltage of 200 kV. Samples were investigated by the means of bright-field TEM, dark field TEM and selected area diffraction (SAD).

Interfacial contact resistance

Wang's method [12] was applied to measure the interfacial contact resistance of samples. In brief, the sample was sandwiched between two carbon papers (Tory 120) and further sandwiched between two copper plates. A constant current was applied onto this assembly cell through the copper plates. By measuring the voltage drop of this cell, the total resistance can be calculated. A micro-ohm meter was used to apply the current and present the resistance directly. To eliminate the

Table 2. Parameter setting of multistep ASPA(N + Nb) treatments.

	Step 1		Step 2	
Sample label	Time (h)	Bias (% of 15 kVA)	Time (h)	Bias (% of 15 kVA)
Bias 0% + 10%	10	0	10	10
Bias 5% + 10%	10	5	10	10

influence of the back side, gold coating was applied on it, so the resistance could be neglected. The detailed calculation process of ICR values can be found in [10].

Corrosion tests

The corrosion behaviour of the untreated and ASPA (N + Nb)-treated 316 SS samples was characterized by potentio-dynamic polarization tests. A standard three electrode system was employed in the tests. A platinum rod, a saturated calomel electrode and the measured sample were acted as the counter electrode, the reference electrode and the working electrode, respectively. A Gamry electrochemical workstation was used to measure and record the corrosion data. To simulate the working environment of proten proton exchange membrane fuel cell (PEMFC), a sulphuric acid aqueous solution (0.5 M H_2SO_4 + 2 ppm hydrofluoric acid (HF)) was selected as the corrosion solution. Before the potentio-dynamic polarization, an open circle potential test was conducted for 1 h to stabilize the sample in corrosion solution. For each sample, three measurements were conducted to verify the reproducibility.

Results and discussion

Surface morphology

The low and high magnification surface morphology SEM images of the ASPA(N + Nb)-treated sample are shown in Figure 1. From the low magnification image (Figure 1(a)) of the Bias 0% + 10% sample, it can be seen that the surface is smooth. On contrary, surface relief, which is one of the distinguishing feature of S-phase [13,14], can be clearly found from the surface of the Bias 5% + 10% sample (marked by yellow arrows in Figure 1(b)) under low magnification. The difference in surface morphology can be confirmed by the surface roughness of these two samples. The surface roughness of the Bias 0% + 10% sample was 0.01 μm, which was similar with that of the untreated surface. While for the Bias 5% + 10% sample, its roughness was around 0.11 μm, which was much higher than that of the former. The high magnification surface morphology SEM images of the ASPA(N + Nb)-treated sample are shown in Figure 1(c,d). The surfaces of both samples were covered by a layer of fine particles. Difference was hardly found from the comparison between these two surfaces, expect that the particle size of the Bias 5% + 10% sample was slightly smaller. The surface composition of ASPA(N + Nb)-treated samples with changing bias is presented in Figure 1(e). Owing to the larger interaction volume of EDS measurement, the obtained results not only revealed the element contents from the surface, but also the sub-surface region. The nitrogen and niobium content of the Bias 5% + 10% sample

was obviously higher than that of the Bias 0% + 10% sample, which might be due to the higher applied bias in the first step.

Layer structures

The cross-sectional SEM images of the ASPA(N + Nb)-treated sample with changing bias are shown in Figure 2. For the Bias 0% + 10% sample (Figure 2(a)), only a deposition layer can be observed, no other layer can be found underneath it. In addition, it is clearly seen that the deposition layer exhibited a columnar structure. In terms of the Bias 5% + 10% sample (Figure 2(b)), a duplex-layer structure can be observed, consisting a deposition layer and a layer underneath. From the GDS element depth profiles shown in Figure 2(c,d), it can be confirmed that both of the deposition layers of two samples were rich in niobium and nitrogen. The underneath layer of the Bias 5% + 10% sample had a higher nitrogen content than that of the Bias 0% + 10% sample. From the XRD results in Figure 2(e), peaks of S-phase can only be found from the spectrum of the Bias 5% + 10% sample, which was in agreement with the previous research [11]. The thickness of the deposition layer and the S-phase layer are listed in Figure 2(f). Beside the difference in the S-phase layer, the deposition layer of the Bias 5% + 10% sample was slightly thicker than that of the Bias 0% + 10% sample.

Owing to the relatively high background of XRD spectrum (Figure 2(e)), phases with low intensity cannot be detected precisely. Therefore, the duplex-layer structure of the Bias 5% + 10% sample was further investigated by the means of TEM. The TEM image and the corresponding SAD patterns of the deposition layer of the Bias 5% + 10% sample are shown in Figure 3. From the TEM bright-field image (Figure 3 (a)), the deposition layer can be easily distinguished from the underneath S-phase layer and its thickness was in agreement with the cross-sectional SEM observation (Figure 2(c)). No cracks or pores can be found from the interface, revealing the sound bounding between the deposition layer and the S-phase layer. The SAD patterns, taken from the deposition layer (Figure 3(b)), displayed several diffraction rings, indicating the polycrystalline structures of the deposition layer. In the SAD patterns, the diffraction patterns of NbN were strong and clear, whereas the diffraction patterns of Fe₃N were very weak, demonstrating that the dominant constituent of the deposition layer was NbN. Because of the usage of Cu Kα radiation to characterize Fe-based materials, fluorescence radiation occurred and resulted in high background in the XRD spectrum. Owing to the relatively small amount of nitrides compared with the stainless steel substrate and the S-phase, the XRD peaks of the former were significantly lower than those of the latter and difficult to
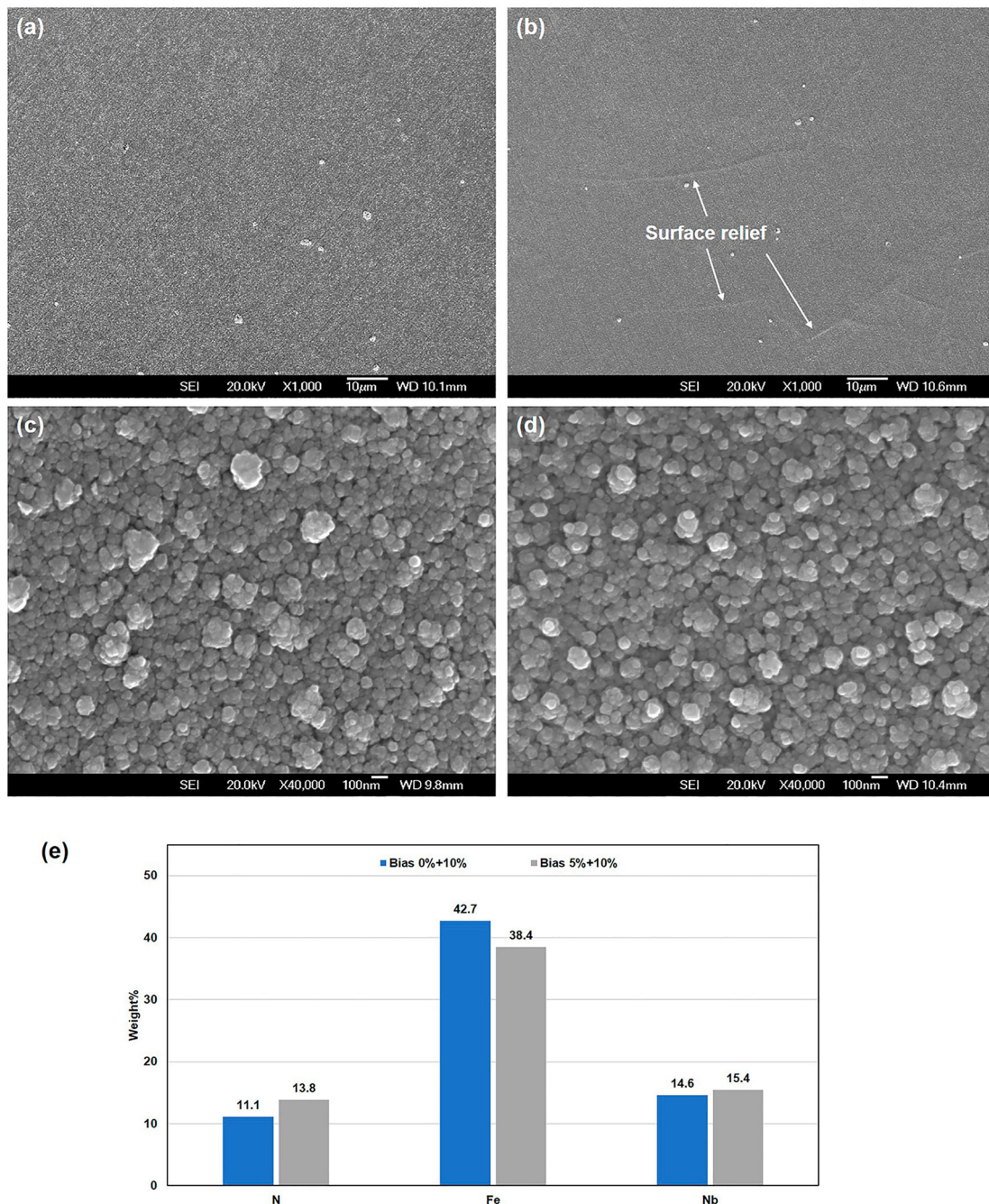
Figure 1. Surface morphology SEM images of ASPA(N + Nb) treated samples: (a,c) low/high magnification of sample Bias 0% + 10%, (b,d) low/high magnification of sample Bias 5% + 10% and (e) surface element content of different samples.

detect among the high background (Figure 2(e)). The EDS tests were also conducted when doing the TEM observation. Three different positions (marked by red circles in Figure 3(c)) were selected to conduct the EDS measurement, namely the centre of the deposition layer (Spectrum 1), the transition zone between the deposition layer and the S-phase layer (Spectrum 2) and the S-phase (Spectrum 3). The atomic percentage of Nb and N exhibited the same trend which was in the order of Spectrum 1 > Spectrum 2 > Spectrum 3, and the atomic percentage of Fe showed the reverse order (Figure 3(d)). This trend of chemical composition was consistent with the GDS element depth profiles as shown in Figure 2(d). The compositional

gradients can greatly enhance the adhesion strength between layers, contributing to the improvement of the corrosion resistance [15], thermal stability [16] and reduction of interfacial contact resistance [17].

Electrical and corrosion performances

The ICR values of ASPA(N + Nb)-treated samples with changing bias are given in Figure 4(a). It can be seen that both of the ICR values were lower than the DOE target of 10 mΩ cm². The Bias 5% + 10% sample with the duplex-layer structure exhibited about 12.2% lower ICR value than the Bias 0% + 10% sample with the single-layer structure. The finding confirms that
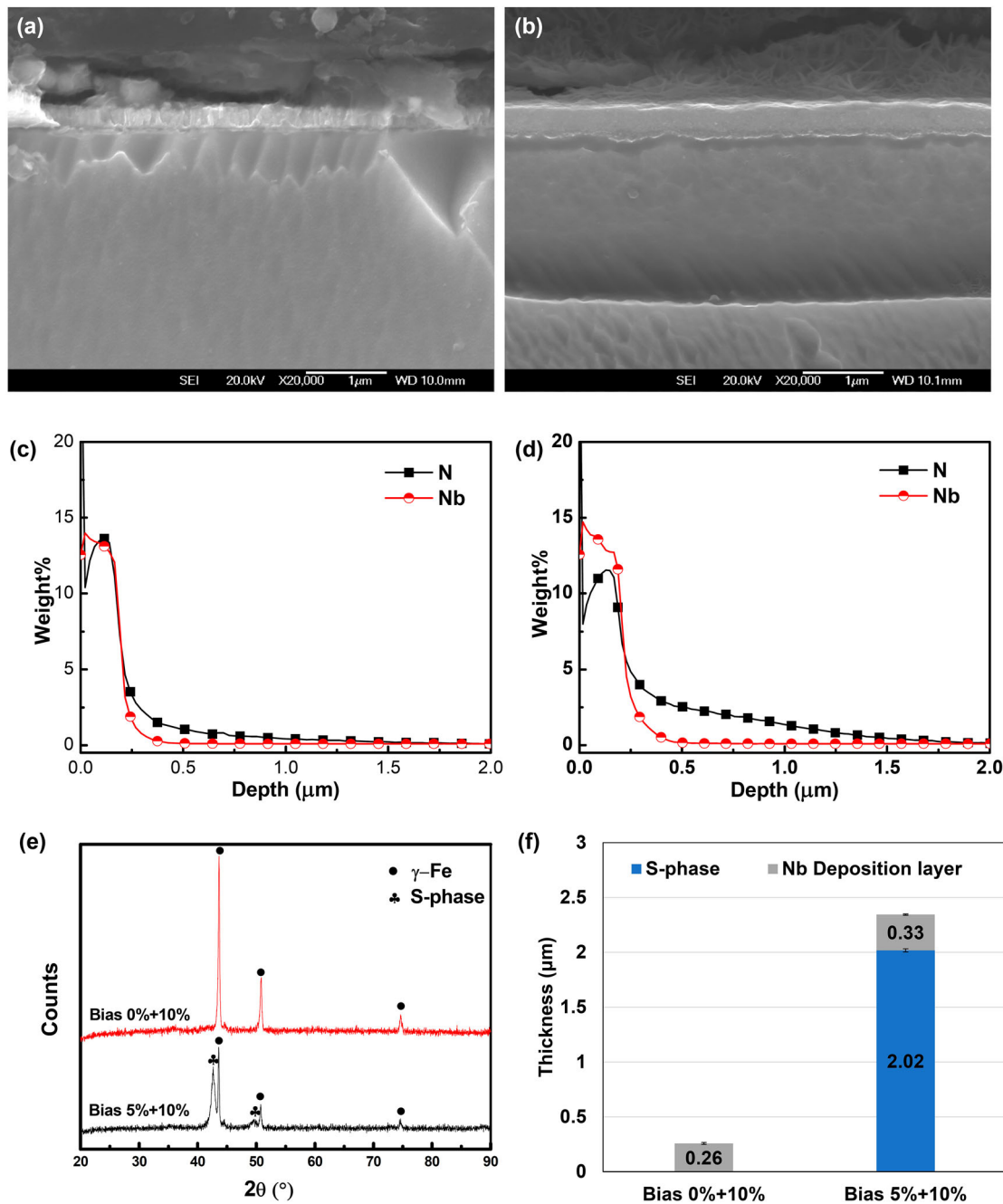
Figure 2. Cross-sectional SEM images of ASPA(N + Nb)-treated sample: (a) Bias 0% + 10% and (b) Bias 5% + 10%; nitrogen and niobium depth profiles of (c) Bias 0% + 10%, (d) Bias 5% + 10%; (e) XRD spectra of samples; and (f) layer thickness of different samples.

the duplex-layer structure has better surface conductivity than that of the single-layer structure. From our previous research [11], the superior electrical conductivity of the duplex-layer structure (deposition layer and S-phase layer) was proved, and the contribution of the NbN deposition layer to the improvement of electrical conductivity was greater than that of the S-phase. In this study, by designing multistep ASPA(N + Nb) with changing applied bias, a duplex-layer structure with a thicker NbN deposition layer was produced and delivered even a lower ICR value than the duplex-layer structure in previous research (8.9 mΩ cm^2). The sound interfacial bonding also contributed to the excellent electrical conductivity.

The potentio-dynamic polarization curves of the ASPA(N + Nb)-treated sample with changing bias are plotted in Figure 4(b), and the corrosion potential and corrosion current density (average values of three measurements) are charted in Figure 4(c). It can be seen that the corrosion potential of ASPA(N + Nb)-treated samples was more positive than that of the untreated sample. The Bias 5% + 10% sample exhibited the highest corrosion potential (−413 ± 1.8 mV), which was 22 and 9 mV higher than the untreated (−435 ± 4.4 mV) and the Bias 0% + 10% samples (−422 ± 5.3 mV), respectively. The corrosion current density of ASPA(N + Nb)-treated samples was lower than that of the treated sample, and the Bias 0% + 10%
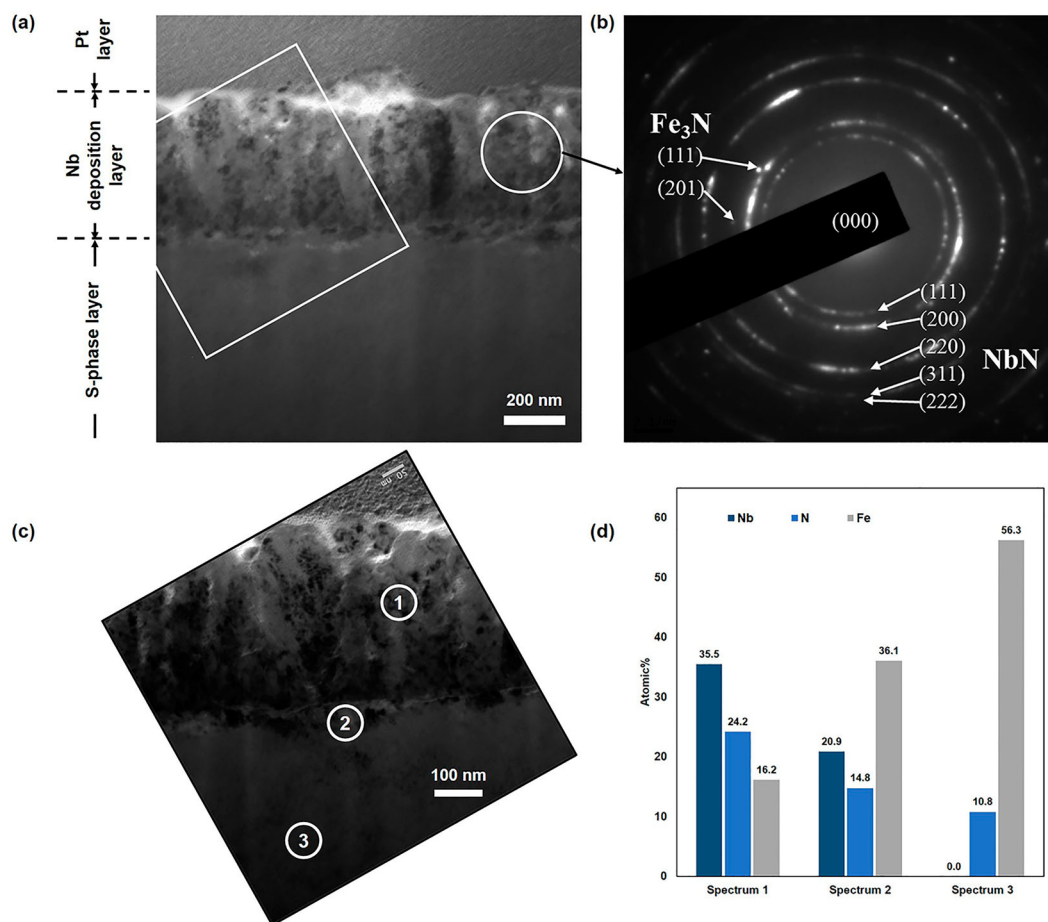
Figure 3. (a) TEM images and (b) SAD patterns of the deposition layer on the Bias 5% + 10% sample; (c) the spectrum position and (d) the EDS results of the red box area in (a).
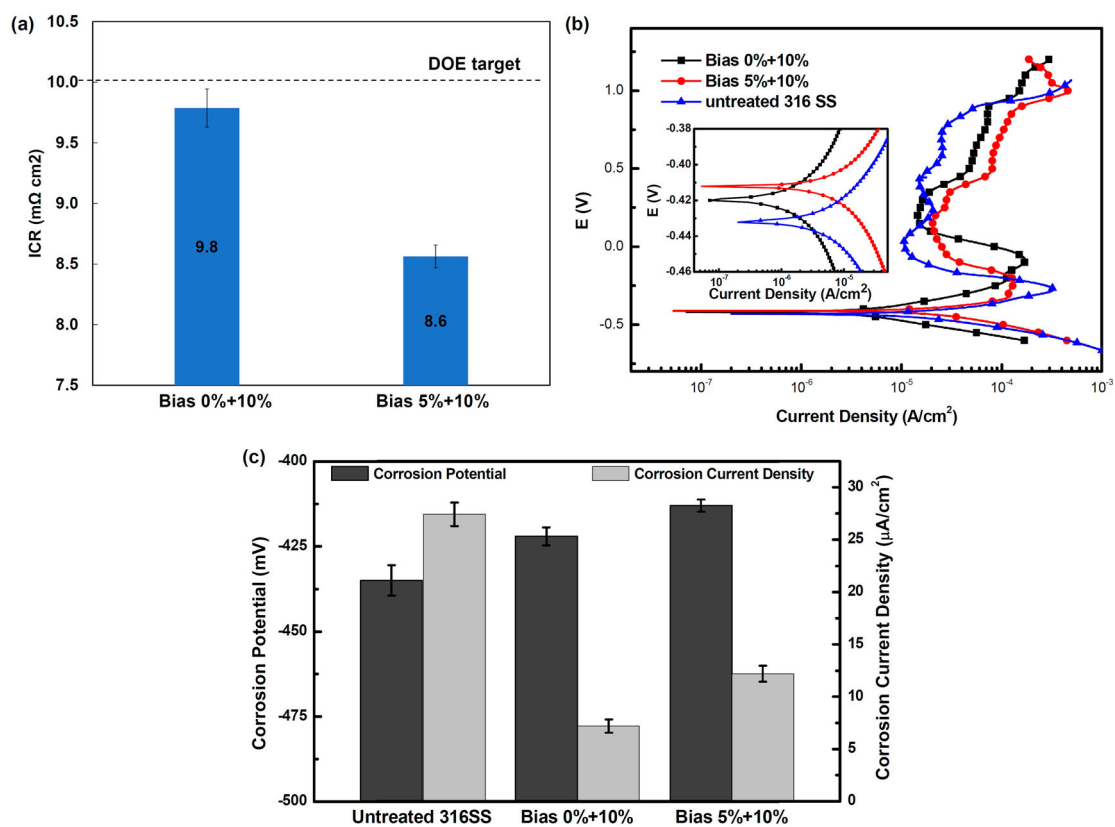

Figure 4. (a) ICR values, (b) potentio-dynamic polarization curves and (c) corrosion potential and corrosion current density of the multistep ASPA(N + Nb)-treated sample.

sample exhibited the lowest corrosion current density. In terms of the current density in the passivation zone, the ASPA(N + Nb)-treated samples showed slightly higher current density than that of the untreated samples, which might be due to the dissolution of Fe_3N in the deposition layer (Figure 3(b)). Comparing the ASPA(N + Nb)-treated samples, the Bias 5% + 10% sample showed higher passive current density than that of the Bias 0% + 10% sample, which might be related with the surface relief found on the surface of the Bias 5% + 10% sample. The surface relief caused by the formation of the S-phase could produce cracks in the deposition layer, thus leading to the relatively high current density [18].

Conclusions

By designing multistep ASPA(N + Nb) treatment with changing bias, the layer structure produced on the surface of 316L stainless steel can be successfully tailored between the single-layer structure and the duplex-layer structure. Through microstructure investigation, the single-layer structure only consisted a dense NbN deposition layer, while the duplex-layer structure consisted a NbN deposition layer and a underneath S-phase layer. For the duplex-layer structure, TEM observation revealed the sound bounding between the deposition layer and the S-phase layer. Performance tests showed that the ASPA(N + Nb)-treated sample with the duplex-layer structure exhibited improved interfacial contact conductivity and higher corrosion potential than the sample with the single-layer structure. The relatively higher corrosion current density of the ASPA (N + Nb)-treated sample can be reduced by the following means: (1) increasing Nb content in the lid of the screen to reduce the content of iron nitride in the deposition layer and (2) increasing the thickness of the NbN deposition layer to provide better protection. In conclusion, multistep ASPA(N + Nb) treatment with changing bias is a promising surface modification method to enhance performances of 316L stainless steel for the application of PEMFC bipolar plates.

Disclosure statement

No potential conflict of interest was reported by the authors.

Funding

References

[1] Zhang H, Jiang K, Qiu Y, et al. Electrochemical properties of niobium and niobium compounds modified AISI430 stainless steel as bipolar plates for DFAFC. Surf Eng. 2019;35:1003–1011.

[2] Wang L, Nam K, Kwon S. Transmission electron microscopy study of plasma nitriding of electroplated chromium coating. Appl Surf Sci. 2003;207:372–377.

[3] Wang H, Brady MP, Teeter G, et al. Thermally nitrided stainless steels for polymer electrolyte membrane fuel cell bipolar plates. J Power Sources. 2004; 138:86–93.

[4] Buhagiar J, Dong H, Bell T. Low temperature plasma surface alloying of medical grade austenitic stainless steel with carbon and nitrogen. Surf Eng. 2007;23:313–317.

[5] Tian R, Sun J, Wang J. Study on behavior of plasma nitrided 316L in PEMFC working conditions. Int J Hydrogen Energy. 2008;33:7507–7512.

[6] Feng K, Kwok DTK, Liu D, et al. Nitrogen plasma-implanted titanium as bipolar plates in polymer electrolyte membrane fuel cells. J Power Sources. 2010;195:6798–6804.

[7] Dong H. S-phase surface engineering of Fe-Cr, Co-Cr and Ni-Cr alloys. Int Mater Rev. 2010;55:65–98.

[8] Li CX. Active screen plasma nitriding – an overview. Surf Eng. 2010;26:135–141.

[9] Li CX, Georges J, Li XY. Active screen plasma nitriding of austenitic stainless steel. Surf Eng. 2002;18:453–457.

[10] Lin K, Li X, Sun Y, et al. Active screen plasma nitriding of 316 stainless steel for the application of bipolar plates in proton exchange membrane fuel cells. Int J Hydrogen Energy. 2014;39:21470–21479.

[11] Lin K, Li X, Tian L, et al. Active screen plasma surface co-alloying of 316 austenitic stainless steel with both nitrogen and niobium for the application of bipolar plates in proton exchange membrane fuel cells. Int J Hydrogen Energy. 2015;40:10281–10292.

[12] Wang H. Stainless steel as bipolar plate material for polymer electrolyte membrane fuel cells. J Power Sources. 2003;115:243–251.

[13] Dong H, Qi PY, Li XY, et al. Improving the erosion-corrosion resistance of AISI 316 austenitic stainless steel by low-temperature plasma surface alloying with N and C. Mater Sci Eng A. 2006;431:137–145.

[14] Lin K, Li X, Dong H, et al. Nitrogen mass transfer and surface layer formation during the active screen plasma nitriding of austenitic stainless steels. Vacuum. 2018;148:224–229.

[15] Kameneva A, Kichigin V. Corrosion, wear, and friction behavior of a number of multilayer two-, three- and multicomponent nitride coatings on different substrates, depending on the phase and elemental composition gradient. Appl Surf Sci. 2019;489:165–174.

[16] Lin H, Liang W, Jia Y, et al. Effect of Al–Y gradient coating on hot corrosion resistance of γ-TiAl alloy at different temperatures. Appl Surf Sci. 2019; 487:868–875.

[17] Demeneva NV, Kononenko OV, Matveev DV, et al. Composition-gradient protective coatings for solid oxide fuel cell interconnectors. Mater Lett. 2019;240:201–204.

[18] Lin K, Li X, Tian L, et al. Active screen plasma surface co-alloying treatments of 316 stainless steel with nitrogen and silver for fuel cell bipolar plates. Surf Coatings Technol. 2015;283:122–128.